Combustion and Flame 265 (2024) 113485

Contents lists available at ScienceDirect

Combustion and Flame

journal homepage: www.sciencedirect.com/journal/combustion-and-flame

Resolving emission factors and formation pathways of organic gaseous compounds from residential combustion of European brown coal

Anni H. Hartikainen [a,*], Satish Basnet [a], Pasi Yli-Pirilä [a], Mika Ihalainen [a], Sini Talvinen [b], Jarkko Tissari [a], Santtu Mikkonen [a,b], Ralf Zimmermann [c,d], Olli Sippula [a,e]

[a] Department of Environmental and Biological Sciences, University of Eastern Finland, FI-70211, Kuopio, Finland
[b] Department of Technical Physics, University of Eastern Finland, Kuopio, FI-70211, Finland
[c] Joint Mass Spectrometry Centre, Helmholtz Zentrum München, DE-85764, Neuherberg, Germany
[d] Department of Analytical and Technical Chemistry, University of Rostock, DE-18059, Rostock, Germany
[e] Department of Chemistry, University of Eastern Finland, FI-80101, Joensuu, Finland

ARTICLE INFO

Keywords:
Residential combustion
Volatile organic compounds
Organic gaseous compounds
Coal combustion
Factor analysis
Air pollution

ABSTRACT

Residential combustion of brown coal can be an important source of ambient air pollution in areas with abundant brown coal deposits, such as Eastern Europe or China. The exhaust emission contents may vary regionally depending on the fuel composition, calling for detailed characterization of emissions from different coal types. In this work, the organic gaseous emissions of European brown coal combusted in a modern chimney stove -type residential appliance were measured by a proton transfer reaction time-of-flight mass spectrometer. Of three consecutive batches of brown coal briquettes, the first batch produced two-fold emission (144 ± 52 mg/MJ) of organic gaseous compounds (OGCs) compared to the later batches (71 ± 35 mg/MJ). The compositions between the batches were, however, relatively similar. Carbonyls accounted for 36 ± 3.0% of the identified emission factors, while aromatic hydrocarbons and oxygenated aromatic compounds contributed 19 ± 3.4% and 16 ± 1.8%, respectively. The complex and overlapping chemical processes within batch combustion were exposed by non-negative matrix factorization, giving insight into the temporal variation in the formation pathways of the OGCs. The OGCs were separated into five factors revealing the chemical fingerprints of the main processes leading to formation of, for example, substituted or single-ring aromatic hydrocarbons. Oxygenated aromatic compounds were related to a distinct factor, which was proposed to form specifically from decomposition of the lignin residues of the brown coal. OGCs from brown coal combustion were estimated to have notable secondary particle formation potential: in photochemical conditions, they may double the organic particulate emission, while reactions in dark conditions may lead to excessive nitrophenol formation.

1. Introduction

Residential brown coal combustion has been a significant source of energy in Europe, likely producing significant aerosol emissions to the atmosphere. Although the trend in residential coal combustion in Europe is decreasing [1], it is still widely practiced and may continue also in future in areas with local coal production [2]. Brown coal combustion has been noted to produce higher pollutants per energy unit than combustion of higher-ranking bituminous (“black”) coal, which in turn has higher emissions than anthracite (“hard”) coal, mainly due to the higher volatile contents of the lower coal ranks [3–8]. During solid fuel combustion, organic emissions can be formed both in the primary pyrolysis of the fuel constituents and in secondary reactions occurring in the flame, including recombination and fragmentation processes. Previous studies on the organic gaseous emissions from residential coal combustion have been focused mainly on experimental conditions representing Chinese coal combustion [4–7,9], while the composition of organic gases from European residential coal combustion remain largely uncharacterized. The composition of brown coal is, however, highly region dependent. Because of its low maturity, brown coal may retain notable fractions of cellulose and lignin originating from the coalifying biomass, while hemicellulose remnants are considered scarcer [10–13]. Differences in fuel composition may cause variance also in the characteristics of brown coal combustion emissions [12]. Further, differences

---

* Corresponding author.
E-mail address: anni.hartikainen@uef.fi (A.H. Hartikainen).

https://doi.org/10.1016/j.combustflame.2024.113485
Received 2 July 2023; Received in revised form 9 April 2024; Accepted 24 April 2024

in combustion appliances and the method of their use will influence the emissions from residential coal combustion [9,14,15]. Processing of the coal also influences the emission profile, and the emissions per energy unit may be reduced by briquetting of the raw-coal chunks [3,5,14].

Organic gaseous compounds (OGCs) from residential combustion may cause direct health effects, including irritation or adverse respiratory effects, such as asthma or allergy [16]. They may also participate in the formation of particulate secondary organic aerosol (SOA) in the atmosphere [17]. Specifically, aromatic hydrocarbonaceous and oxygenated aromatic species are considered to generate SOA via reactions with atmospheric oxidants, such as hydroxyl (OH) or nitrate (NO_3) radicals [18–20]. Residential coal combustion produces high amounts of such aromatic organic compounds, although the relative contribution of different species to the total organic gaseous emission likely varies depending on the fuel and combustion conditions [4,6,21]. Furthermore, the OGCs from combustion processes may influence the oxidant availability and reaction pathways in ambient air [22–24].

Solid fuel combustion is a complex process containing thousands of simultaneous reactions which depend on conditions such as fuel composition, temperature, and availability of oxygen [25–27]. Thus, OGCs origin from a range of temporally overlapping reaction pathways. To simplify the characterization of the batchwise residential combustion, the process is often divided into three main 'phases': 1) ignition, where the temperature increases rapidly and moisture and most volatile species evaporate from the fuel, 2) pyrolysis, where organic volatile species in the fuel evaporate and burn with a visible flame in ever-rising temperature, and 3) ember burning phase with low oxygen availability on the fuel and high carbon monoxide emissions. State-of-the-art online mass spectrometers provide high resolution chemical information in relatively time high resolution, enabling improved characterization of the combustion emissions. Factorization of high-resolution mass spectra has been increasingly utilized for describing combustion emissions [28–31], OGC source apportionment [32–35], or evolution of organic gases in ambient air or laboratory setting [36,37]. However, to our knowledge, the use of factor analysis has not been extended to the characterization of the processes driving the formation of OGCs during continuous batchwise solid fuel combustion, which is the typical method of domestic residential heating.

This work characterizes the organic gaseous emission from residential combustion of Lusatian brown coal briquettes (BCB) in a chimney stove, representing typical European conditions of BCB use. The OGCs are measured by a proton transfer reaction time-of-flight mass spectrometer (PTR-ToF). Emission factors for the gaseous species are presented and their SOA formation potential is estimated in order to constrain the impact of the OGC emission of BCB combustion on European air pollution. The temporal progression of the OGC emission formation throughout consecutive combustion of three BCB batches is assessed by the means of non-negative matrix factorization.

2. Material and methods

2.1. Experimental protocol and combustion efficiency

Experiments were conducted in the ILMARI combustion laboratory of University of Eastern Finland (www.uef.fi/ilmari). Commercially available brown coal briquettes (BCB) manufactured from German coal from the Lusatian region (Rekord-Briketts G156; Lausitz Energie Bergbau AG, Germany) were used as fuel. Composition of the BCB is presented in Supplementary Table S1. The combustion appliance was an air-staged, non-heat retaining chimney stove (Aduro 9.3, Aduro A/S, Denmark), which is designed for indoor residential heating. The stove complies with the EN13240 European standard and the NS3058 Norwegian standard. Experimental setup is illustrated in Supplementary Figure S1.

Prior to ignition of the brown coal briquettes (BCB), the stove was preheated by combustion of two (experiments 1, 2, and 6) or three (experiments 3–5) batches of spruce logs. This is in accordance with the instructions of the appliance and fuel providers and reflects the normal use of coal fuels in small-scale appliances. Based on the flue gas temperatures measured from the stack, the degree of preheating was similar for all experiments (Supplementary Figure S2). Flue gas temperatures were the highest directly following the spruce combustion, as wood fuels have a higher volatile content than brown coal (based on proximate analysis), leading to higher combustion rate, larger flames, and eventually higher flue gas temperatures.

BCB was combusted for three consecutive 1 h batches, each consisting of three briquettes (á 0.58 kg). The briquettes were arranged in grate direction tightly parallel to each other. The briquettes were placed on top of the residual chars from spruce (first batch) or BCB (second and third batches) combustion to ease their ignition. The remaining charcoals may thus have impacted the OGC emission of the subsequent batch. However, organic emissions from batchwise combustion are mainly formed during ignition and flaming combustion, with typically low emission from the residual char combustion as vast majority of the fuel volatile content has then already been released [31,39]. After the 1st hour of the 2nd and 3rd batch the embers were stoked, and ember burnout periods of 20 min and 40 min took place before the addition of 3rd batch and after the 3rd batch, respectively.

The combustion efficiency during experiments can be considered good for a batchwise operated solid fuel combustion appliance. Carbon monoxide was emitted mainly during the ignition of the batch, leading to average (harmonic mean) modified combustion efficiencies (MCE, calculated by Eq. (1) from the raw gas concentrations) of 0.95, 0.96, and 0.97 for the first, second, and third batches, respectively, when the ember burnout phases are excluded.

$$MCE = \frac{CO_2}{CO_2 + CO} \tag{1}$$

The good combustion conditions were achieved by the relatively modern, state-of-the-art combustion appliance in use and the extensive prewarming of the combustion chamber, which was confirmed by the measurement of the flue gas temperatures from the stack. Air-to-fuel ratios (λ) were calculated as (Eq. (2)):

$$\lambda = \frac{CO_{2,\ stoic}}{CO_{2,\ dry}} \tag{2}$$

where $CO_{2,\ stoic}$ is the CO_2 concentration in dry exhaust from stoichiometric combustion of the brown coal briquettes (19.5%) and $CO_{2,\ dry}$ the measured CO_2 concentration in dry air. λ ranged roughly from 2 to 5, leading to adiabatic combustion temperatures varying between 1300 ℃ and 600 ℃. In batchwise solid fuel combustion, however, the amount of excess air varies spatially, and a high variability in temperatures is expected within the combustion chamber. MCEs, flue gas temperatures, λ, and the range of adiabatic temperatures are shown in Supplementary Figure S2. The overall setup, combustion conditions, and the general composition of the exhaust emissions from BCB combustion have been priorly discussed by [21] and [38].

2.2. Sampling and exhaust gas measurements

Exhaust was sampled from the stack with a heated probe using a PM_{10}-precyclone followed by a two-stage diluter system consisting of a porous tube diluter (Venacontra, Finland) and an ejector diluter (DI-1000, Dekati, Finland). The sample was externally diluted with clean, room-temperature air (AADCO) by a dilution ratio (DR) of 30. DR of 60 was applied for the first 10 min of the 1st BCB batch due to the high emission concentrations. The undiluted exhaust gases were measured by a Fourier Transform Infrared Analyzer (FTIR; Gasmet Technologies Ltd., model DX4000, Finland). The FTIR was calibrated towards CO_2, CO, NO_x, CH_4, methanol, and a range of other compounds typical for small scale combustion, which have been discussed in detail elsewhere [21, 40]. Concentration of CO_2 in the diluted exhaust were measured by single gas analyser (ABB).

2.3. Proton transfer reactor mass spectrometry

The organic gases in the exhaust were quantified by a proton transfer reactor time of flight mass spectrometer (PTR-TOF 8000, Ionicon Analytik, Austria [41]). H_3O+ was used as the primary ion, resulting in observation of compounds with proton affinity higher than that of water (691 kJ/mol). These compounds include the majority of volatile oxygenated and aromatic organic compounds while the detection of, for example, small alkanes is limited due to their low proton affinity. A two-point mass calibration was performed using isotope of H_3O+ ($H_3^{18}O+$, m/z 21.02) and 1,3-diiodobenzene (m/z 203.94), which was input alongside the exhaust sample. The ratio of electric field to gas number density (E/N) in the instrument was 121 – 123 Townsend. The instrument was operated at 8 s time resolution. Compound specific reaction rates with H_3O+ in the PTR-ToF drift tube were applied when available (Supplementary Table S2) [42]. A reaction rate of 2×10^{-9} cm^3/s with H_3O^+ was assumed for the rest of the ions.

Proton transfer is a relatively soft ionization method, and fragmentation of the identified compounds in the PTR-ToF is considered minor and was not corrected for. However, fragments of larger compounds may influence specific m/z's. For example, hydrocarbon signals at m/z's 43 and 57 may origin from larger alcohol or aromatic structures [43,44], while the signal of benzene (C_6H_6—$H+$, m/z 79.05) may be enriched by fragments of larger aromatic structures [44,45].

2.4. Data processing

The CO_2 concentrations in the dry diluted exhaust ($CO_{2,\ diluted}$) and in the background air ($CO_{2,\ bg}$) were utilized to calculate stoichiometric correction factors (SCF, Eq. (3)) to account for both the external dilution (DR 30) and the internal dilution of the combustion process, i.e., excess air in the exhaust. SCFs are displayed in Supplementary Figure S2.

$$SCF = \frac{CO_{2,\ stoic} - CO_{2,\ bg}}{CO_{2,\ diluted} - CO_{2,\ bg}} \tag{3}$$

The background corrected exhaust concentrations were converted to emission factors (EFs) by unit of embodied energy following Eq. (4).

$$EF = c_n \times SCF \times Q_s \times k \tag{4}$$

where c_n is the volume concentrations in dry flue gas, Q_s is the stoichiometric dry volume of flue gas produced in combustion of the briquettes (0.25 m^3/MJ), and k is the fuel moisture correction factor (1.015 for the brown coal briquettes with moisture content of 14.4%). The net calorific value of the briquettes was 24 MJ/kg in dry mass basis.

Batchwise averaged EFs were calculated for the full 1 h batches, so that the ember-phase after stoking was excluded. Compounds with average EFs exceeding a threshold of 0.1 mg/MJ in at least one batch were considered in further analysis. This limit corresponds to roughly 0.5 ppb at the m/z 40 and 0.1 ppb at the m/z 180 for the diluted exhaust gas measured by the PTR-ToF.

2.5. Characterization of OGCs

Chemical formulas were assigned to ions based on their mass-to-charge-ratios (m/z). Each ion may include several isomers, which can't be resolved based on the molecular formulae alone. Thus, the ions were identified and grouped based on the assumed chemical composition (Table S2). Molecular formulas were used also for the estimation of the saturation mass concentrations (C_0) using the parametrization by Li et al. [46]. It should be noted, however, that the true C_0 depends on the functional groups, which cannot be discerned based on the molecular formulae. Organic aerosols are often characterized by their average carbon oxidation state (OS_C), which was estimated for the identified ions as $OS_C = 2 \times n_O / n_C - n_H / n_C$ [47]. The degree of unsaturation of the detected ions was estimated based on their double bond equivalents ($DBE = n_C - (n_H/2) + (n_N/2) + 1$), which describe the total amount of double bonds and ring structures in the molecule. n_O, n_C, n_H, and n_N are the numbers of oxygen, carbon, hydrogen, and nitrogen in the molecule, respectively. Compounds with DBE $\geq$ 4 were classified as aromatic, with further separation between aromatic hydrocarbons and oxygenated ions based on molecular formula. Furans, a distinct group of oxygenated cyclic compounds containing a five-membered aromatic ring, were classified separately.

2.6. SOA yield estimation

A bottom-up estimation of the SOA formation potential of the emission in photochemical conditions was generated using literature SOA yields of specific OGCs. This estimation includes the potential precursors for which literature yields are available; see Section 1 of the Supplementary Material for more details. SOA formation potential of OGCs depends on existing conditions, such as humidity, availability of NO_x, and particle concentrations in the air. For the bottom-up estimation, PM concentration of 20 μg/m^3 was assumed to reflect typical European conditions [48]. In general, higher SOA yields have been measured in NO_x limited than in NO_x-rich conditions for combustion emissions and for aromatic precursors [23,49,50], although the relationship appears inverse for, e.g., furans [51].

The provided bottom-up estimate does not account for the later stage oxidation of the reacted compounds or the interactions between the different species [23,17]. Further, the chemistry within the particulate aerosol is overlooked, leading to underestimation of oligomerization and other heterogeneous accretion reactions [49,52,53]. Thus, this estimation can be considered as a low limit for the SOA formation potential. However, providing a ballpark estimate on the extent of the SOA formation is valuable for the consideration of the impact of BCB combustion on ambient air quality.

2.7. Statistical methods

The temporal emission profiles obtained from the PTR-ToF during BCB combustion were assessed by means of non-negative matrix factorization (NMF) [54]. NMF reduces the dimensions of the high-resolution spectra by approximating the original n x m matrix by two solution matrices with sizes n x k and k x m, where k is the number of factors. The interpretation of the results is simplified by constraining the solutions to non-negative values. The NMF algorithm is inherently similar to the positive matrix factorization (PMF) algorithm, but in contrast to PMF or some other popular factorizing methods, NMF algorithms make no assumptions of the measurement errors [55]. The analyses were performed with the MATLAB function nnmf [56] using the stoichiometrically corrected timeseries of molar fractions. Residual char burning phase was excluded from the NMF analysis to not overweigh the minor emissions from ember burning. To confirm the robustness of our results, NMF was applied with two algorithms, alternating least squares and multiplicative update, which produced similar outcomes. NMF was applied to both the original time resolution (8 s) and for averaged data (1 min). As all applications led to analogous conclusions, only the results obtained from the original time resolution with the alternative least squares algorithm are shown.

Mann-Whitney *U test* was used for testing whether the differences between the 1st and later batches were statistically significant. Significance level of $p = 0.05$ was used as a limit to reject the null hypothesis for the statistical tests. Batchwise averaged results are reported as arithmetic means of batchwise averages ± standard deviation of the batch averages.

3. Results and discussion

3.1. Emission factors

A total of 120 ions with average EF exceeding 0.1 mg/MJ in at least one batch were identified from the PTR-ToF spectra between *m/zs* 40 and 200 (Fig. 1a-b; Table S2). All these compounds can be classified as either volatile organic compounds (VOCs, saturation mass concentration $C_0 > 10^6$ μg/m^3) or intermediate VOCs (IVOCs, 10^3 μg/m$^3 < C_0 < 10^6$ μg/m^3) (Fig. 1c), meaning that they reside predominantly in the gaseous phase in the experimental and ambient conditions. The share of IVOCs to the total observed EF was 13 – 19%.

The total average OGC EF of the first batch was 144 ± 53 mg/MJ, which was roughly a factor of two higher than the EF of the later batches (in total 71 ± 35 mg/MJ; 61 ± 16 mg/MJ and 81 ± 48 mg/MJ for the second and third batch, respectively). In fuel mass basis, the EFs were 3.52 ± 1.29 g/kg, 1.50 ± 0.39 g/kg, and 2.29 ± 1.37 g/kg for 1st, 2nd, and 3rd batch, respectively. It should be noted that the PTR-ToF analysis does not include lightweight alkanes, which were evidently emitted with EFs close to that of aromatics, as measured by the FTIR directly from the stack [21]. The highest concentrations were always emitted at the ignition of each batch (Fig. 2), as is typical for batchwise residential combustion when the starting temperature is high enough to rapidly degrade several types of chemical bonds in the fuel, leading to release of volatile species in high quantities.

The formation of emissions was slower for the first batch than the later batches, during which the EFs remained relatively low after the first 15 min. The first batches were ignited from residues of spruce charcoals, and as wood has a higher volatile content than brown coal, less char residue remained for the ignition of the first batch than for the subsequent batches. The lower charcoal amount led to slower ignition and consequently increased the amount of OGC emissions for the first BCB batch compared to the later ones. The similarity of the emissions of the second and third batches, however, indicates that OGC emissions of the subsequent batch were not significantly influenced by having a prolonged 20 min burnout of BCB charcoals prior to new batch addition.

These results are specifically representative of European conditions, which may crucially differ from other regions due to regionally different coal fuel compositions and heating appliances. The use of a modern combustion appliance was very likely to decrease the OGC EFs in comparison to traditional coal burners or cookstoves. Indeed, the observed EFs are an order of magnitude lower than total gaseous organic carbon emission (including methane) observed for BCB combustion in hot-water boilers [14]. Further, the briquetting of the brown coal was likely efficient in decreasing the EFs, which were similar to those previously measured for Chinese bituminous coal chunks [4–7] or Indian residential charcoal burning [57] but notably higher than previously observed for anthracite [4,7] or briquetted bituminous coals [5,7]. The OGC EFs of residential BCB combustion exceed those of brown coal combustion in larger power plants by roughly two orders of magnitude [58], being in the same range with residential wood log combustion [59,60].

3.2. Properties of the OGCs from brown coal combustion

The compositions of the organic gaseous emission were roughly similar for all batches (Pearson correlation coefficients of 0.97 – 0.98 between the average spectra), despite the two-fold differences in the EFs between first and later batches. This also indicates that the spruce embers remaining in the firebed at the ignition of the first BCB batch had no major impact on the emissions. The observed ions had average carbon oxidation states ranging from −2 to +2, with the mainly acidic

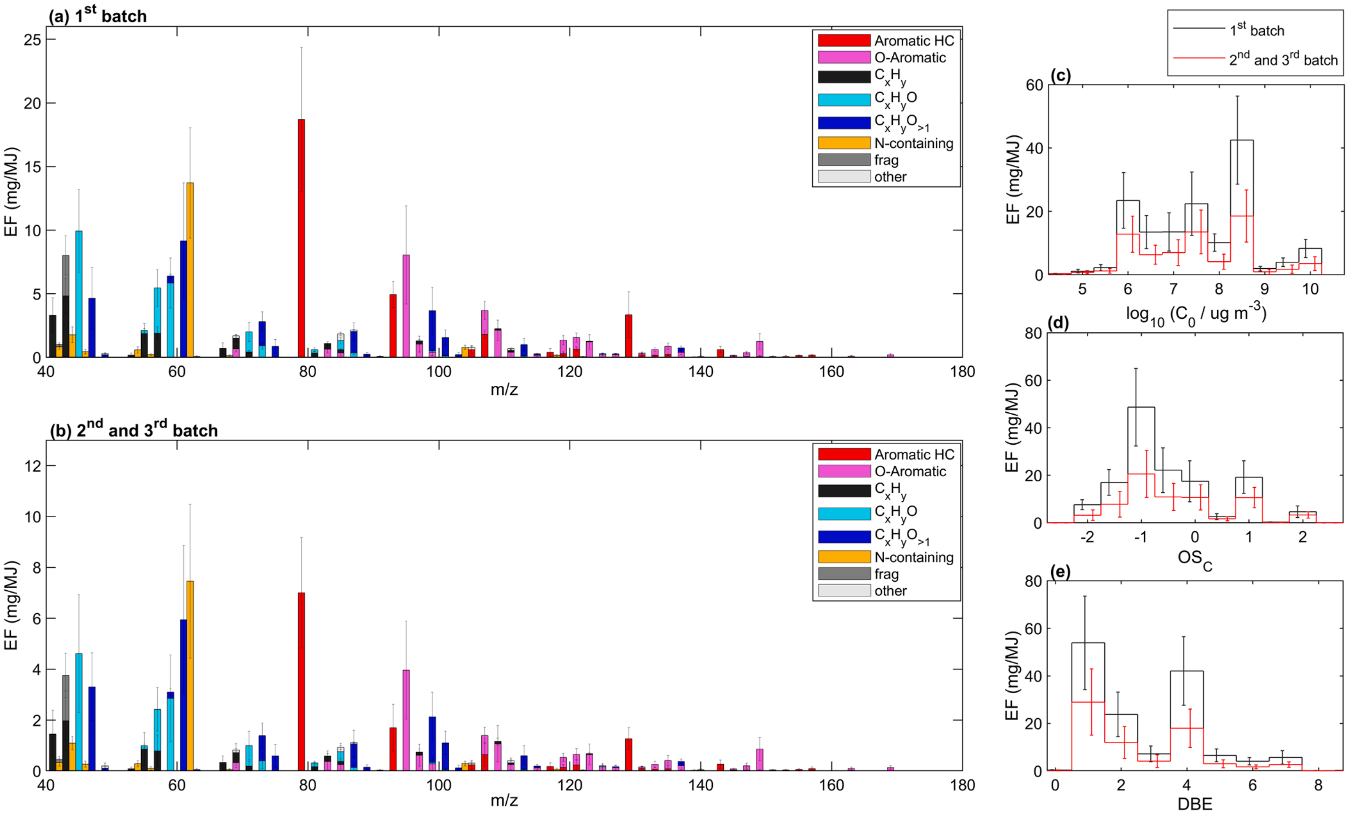

Fig. 1. Average spectra of the ions observed by PTR-ToF: absolute emission factors (EFs) (a-b) and the EFs distributed by saturation mass concentrations (c; bin width 0.5), average carbon oxidation states (d; bin width 0.5), and double bond equivalents (e; bin width 1). Error bars denote the standard deviation of the batchwise averaged means. Note that the high-resolution mass spectra in (a) and (b) are illustrated in unit mass resolution for simplicity, and ions at the same unit mass are stacked.

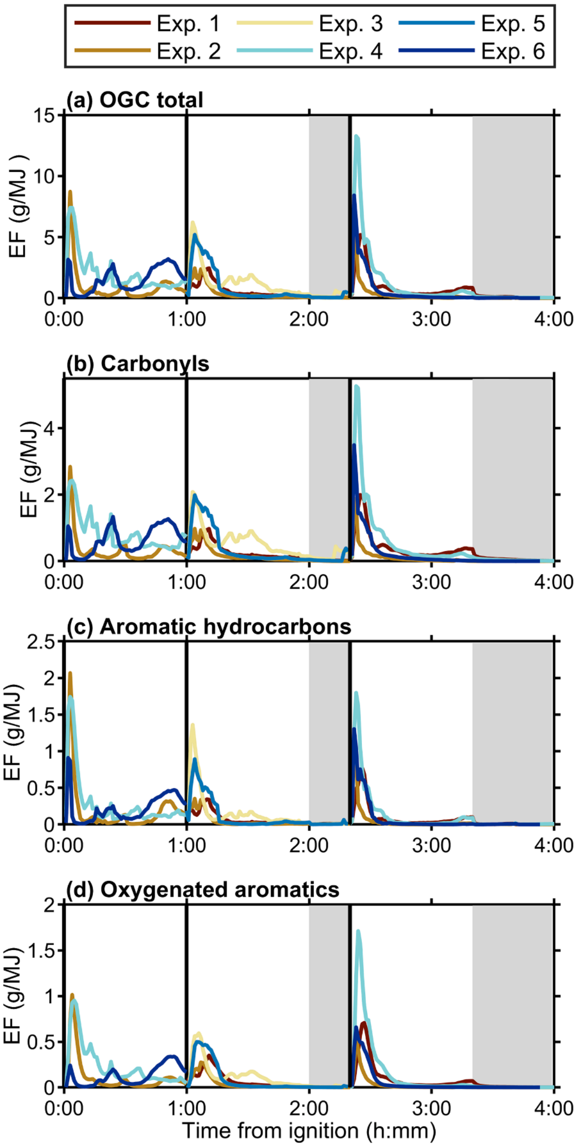

Fig. 2. Emission profiles during the six BCB experiments (Exp. 1–6). Emission factors (EFs) are shown for the sum of the OGCs (a), carbonyls (b), aromatic hydrocarbons (c), and oxygenated aromatics (d). Horizontal lines indicate the addition of new batch. The stoking periods (in grey) were excluded from the calculation of average EFs.

compounds with positive OS_C forming 11 ± 2% of the EF (Fig. 1d). The $n_O:n_C$ -ratio was slightly but statistically significantly (one-tailed Mann-Whitney *U test* $p = 0.03$) lower for the first batches (0.27 ± 0.03) compared to later batches (0.34 ± 0.04), while $n_H:n_C$ -ratios were similar for all batches (1.36 ± 0.03, two-tailed Mann-Whitney *U test* $p = 0.55$). The resulting batch-wise averaged OS_Cs were on average −0.39 ± 0.15 for the total emission, with a small and statistically unsignificant differences between first and later batches (−0.52 ± 0.05 for first, −0.34 ± 0.15 for later batches; one-tailed Mann-Whitney *U test* $p = 0.07$).

The total $n_o:n_C$ -ratios in the exhaust were notably higher than previously assessed for residential combustion of bituminous coals with PTR-ToF (0.07 – 0.08, respectively, when taking into account the similar *m/z* range of 40 – 200 [4]). Coalification process in general increases the carbon content and decreases the oxygen content in the coal [13], likely decreasing the oxygenated organic emission as well. For anthracite, n_o:n_C -ratios have, however, previously been in the range of (0.17 – 0.36), with the abundance of isocyanic acid (HCNO) increasing the ratios [4]. The $n_o:n_C$ -ratios of BCB combustion were similar to previously assessed OGC emissions in fresh logwood combustion exhaust from the same stove [39], but the lower $n_H:n_C$ -ratios led to higher OS_Cs.

3.3. Emissions by functional groups

There were approximately 1.5 – 3 -fold differences between the absolute OGC EFs of the first and later batches (Supplementary Figure S3). However, the relative contribution of the different compound groups remained relatively similar between the three consecutive batches. The EFs of the ions grouped based on functionality are presented in Fig. 3 and Supplementary Table S2.

Aromatic hydrocarbons. 18 of the ions were classified as aromatic hydrocarbons (ArHC; C_xH_y with DBE ≥ 4). The total ArHC EFs were 33 ± 9.8 mg/MJ and 12 ± 5.0 mg/MJ for the first and later batches, respectively, contributing 19 ± 3.4% to the total OGC emission. ArHC were dominated by a few major compounds, namely, benzene (C_6H_6—*H*+, *m/z* 79.05), with EFs of 18.7 ± 5.7 mg/MJ and 7.0 ± 2.2 mg/MJ for first and later batches, respectively, and toluene (C_7H_8—*H*+, *m/z* 93.07), with EFs of 5.0 ± 1.0 and 1.7 ± 0.9 mg/MJ for first and later batches, respectively. It should be noted that the EF of benzene may be slightly overestimated due to fragmentation of larger aromatic compounds in the PTR-ToF. However, the signals for larger aromatics were relatively low compared to the benzene signal, indicating minor

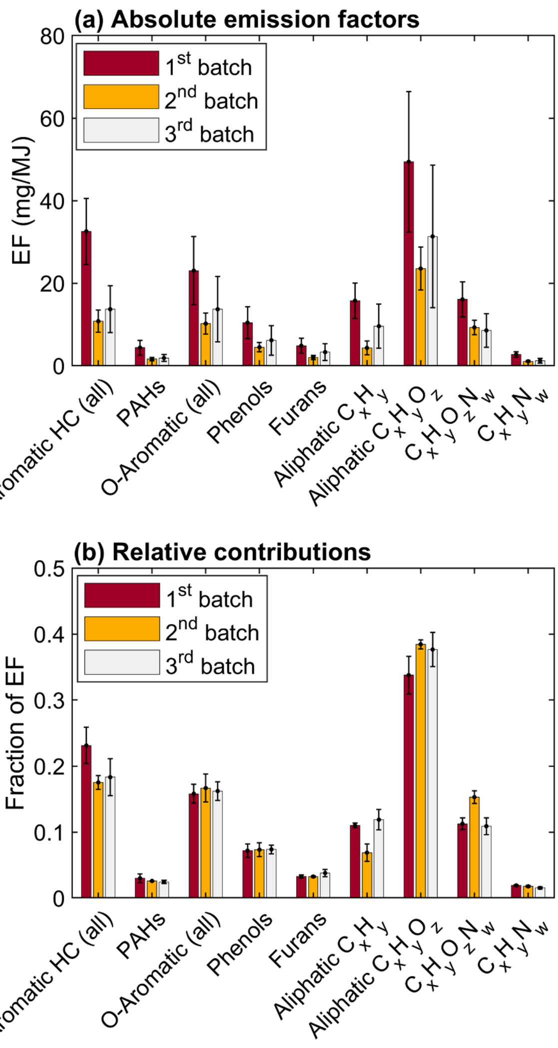

Fig. 3. Average emission factors (EFs) for the OGC groups. The contributions of the different groups are shown as absolute EFs (a) and as fractions of the total EF (b). Error bars denote the range of observed values (minimum-maximum).

interference by other compounds at *m/z* 79.

The PTR-ToF spectra compassed the smallest polycyclic aromatic hydrocarbon (PAH) compounds, namely, naphthalene ($C_{10}H_8$—*H*+, *m/z* 129.07), methylnaphthalene ($C_{11}H_{10}$—*H*+, *m/z* 143.09), and three C12-aromatics. The combined PAH EFs were 4.4 ± 2.2 mg/MJ and 1.7 ± 0.7 mg/MJ for 1st and later batches, respectively, of which naphthalene accounted for the majority (3.4 ± 1.8 mg/MJ and 1.3 ± 0.4 mg/MJ for 1st and later batches, respectively). Because larger PAHs have intermediate volatility, their partitioning to gas phase might be lower in these experimental conditions compared to ambient concentrations with notably greater exhaust dilution.

Oxygenated aromatics. Oxygenated aromatics (O-Ar) comprised in total 34 ions, accounting for a 16 ± 1.8% share of the total EF with EFs of 10.4 ± 4.7 mg/MJ and 5.3 ± 3.0 mg/MJ for the 1st and later batches, respectively. Of individual compounds, oxygenated aromatic exhaust was dominated by phenol (*m/z* 95.05), with EFs of 8.0 ± 3.9 mg/MJ and 4.0 ± 1.9 mg/MJ for the 1st and later batches, respectively. The ratio of O-Ar to ArHC decreased from 1.5 ± 0.15 for the first batch to 1.1 ± 0.23 for the later batches (one-tailed Mann-Whitney *U test* $p = 0.02$). This is contrast to Klein et al.[6], who suggested that the share of oxygenated aromatics in coal combustion exhaust increases with continuous combustion with rising temperature. The temperatures in the flue gas concentrations in the stack, however, indicates no increase in combustion temperature during the consecutive BCB combustion (Supplementary Figure S2). Phenolic compounds are formed in the thermal decomposition of lignin residues in the brown coal [25,61]. The aromatic structures in maturing coal have been noted to progress from substituted, catechol-like structures to phenol-like and finally to hydrocarbonaceous during the continuous coalification process [13]. However, the ratio of O-Ar to ArHC was similar to those previously measured for bituminous coals [4,6]. The lignin composition of brown coal depends on the origin of the coal, which may also influence the phenolic emissions from different brown coals.

Furans. 11 $C_xH_yO_z$ compounds were separately classified as furans. The EF of furans was 4.85 ± 2.25 and 2.65 ± 1.74 mg/MJ for the 1st and later batches, respectively, contributing 3.5% ± 0.47% to the total EF. The most emitted furanoic compounds were benzofuran (C_8H_6O—*H*+, *m/z* 119.05) and furfural ($C_5H_4O_2$—*H*+, *m/z* 97.03). Gaseous furanoic emissions have rarely been quantified for residential coal combustion, and their emission is likely to depend on the coal rank. They are formed through depolymerization of cellulose products, and are a major constituent of the oxygenated carbon fraction of particulate soot [25,62]. The furanoic EFs and their share of the total organic gaseous emission were notably higher for the BCB combustion than previously observed for higher ranking coals [4]. Rather, the furanoic emissions per energy basis were higher or in the same range as previously observed for residential biomass burning [20,60]. This implies that the emissions from persistent residential brown coal burning may obstruct the use of furans as markers for biomass burning [63].

Oxygenated aliphatic compounds. Aliphatic oxygenated compounds formed a major share (37 ± 3.1%) of the emission. 36 ± 3.0% of the total EF could be classified as carbonylic based on the most probable assignments of the observed ions. Acetaldehyde (C_2H_4O—*H*+, *m/z* 45.03), formic acid (CH_2O_2—*H*+, *m/z* 47.01), and acetic acid/glycoaldehyde ($C_2H_4O_2$—*H*+, *m/z* 61.03) were the most important individual carbonyls with shares of 6.6 ± 0.5%, 4.3 ± 1.1%, and 7.7 ± 1.3% of the total EFs, respectively. These compounds may originate from the lignin or cellulose residues of the brown coal, and are also formed in the flame by thermal cracking of larger compounds [25].

Nitrogen-containing OGC. Nitrogen containing emissions consisted mostly of CH_3NO_2—*H*+ (*m/z* 62.02), which accounted for on average 10 ± 2% of the total EF. CH_3NO_2—*H*+ likely represents nitromethane or its isomer methyl nitrite, as it appears connected to reactions of methyl radicals and NO_x [64] with emission coinciding with those of CH_4 and CO (Supplementary Figure S4). CH_3NO_2—*H*+ has also previously been observed from residential coal combustion, although in lower proportion to the total EF [4,6], and has in the past also been observed in the vehicular exhaust emissions [65]. The formation of nitrogen containing organic compounds in such high quantities may have notable implications to the radical chemistry and products in the flame [66,67], and should be considered in the future also in the context of solid fuel combustion.

Gaseous nitroaromatic emission was minor, with nitrophenol EF of 0.06 ± 0.04 mg/MJ. Lower-volatility nitrophenols were likely to have condensed onto the particle phase and thus not visible in the PTR-ToF spectra.

3.4. SOA formation potential of the BCB combustion OGCs

The ambient SOA formation potential of the OGCs from BCB combustion was estimated using literature yield values; see the Supplementary Section S1 for a detailed consideration of this bottom-up estimation. The aromatic hydrocarbons and oxygenated aromatic compounds were evaluated to be the main SOA precursors in the BCB exhaust (Supplementary Figure S5), which is in accordance with previous studies on residential combustion of coal or wood [18–20,68]. In photochemical conditions, the reactions with hydroxyl radicals (OH) drive SOA formation, which was estimated to range 16 – 29 mg/MJ for the first, 4 – 15 mg/MJ for the later batches in NO_x-limited atmosphere (6 – 12 mg/MJ and 2 – 6 mg/MJ with abundant NO_x) (Supplementary Figure S5). These estimated SOA EFs are in the same range as the primary organic particle emission from the BCB combustion (5 – 22 mg/MJ [38]). In other words, the photochemical formation of secondary aerosols from the OGCs may at least double the contribution of BCB combustion to ambient organic particulate matter.

In dark conditions, NO_3 radicals accumulate and dominate the SOA formation [69]. The NO_3 reactivity of phenols and furans is sufficient for their emission to completely react within one night, while aromatic hydrocarbons are relatively stable in the dark. Phenol + NO_3 -reactions lead to formation of nitrophenols [70–72], which effectively partition to the particulate phase in ambient conditions [73]. BCB combustion exhausts were relatively phenol-rich compared to, e.g., wood combustion, for which nitrophenol formation in the dark has been previously established [20], indicating elevated nightly SOA potential for BCB OGCs. Recently, dark SOA yield exceeding 1.1 was found for catechol [74], which has been estimated to produce 4-nitrocatechol SOA in mass yield of 1.2 [71]. In the atmosphere, such nitrophenol-containing SOA is considered so-called ‘brown carbon’, with relatively strong potential to absorb light in the visible wavelengths [72,74,75], potentially increasing the radiative forcing caused by BCB combustion. Previously, freshly emitted particulate nitrophenol EFs from residential coal combustion have been noted to depend on the phenolic content of the fuels, with particulate nitrophenol EFs in the range of 8 – 12 mg/kg for Chinese low-maturity lignite coals [76]. Based on the high phenolic emissions (EFs of 55 – 250 mg/kg in fuel mass basis), the ultimate nitrophenol input from residential combustion of low-rank coal might be even an order of magnitude higher; however, this hypothesis should be verified by well characterized dark aging studies of residential coal combustion exhausts.

3.5. OGC formation pathways

Non-negative matrix factorization (NMF) was applied to the high-resolution mass spectra to provide insight on the temporal variation in the emission formation and on the formation pathways of the OGCs. Altogether five factors were discerned from the OGC timeseries (Fig. 4):

1) Aromatic hydrocarbons connected to fuel pyrolysis
2) Hydrocarbons connected to low combustion efficiency during fuel pyrolysis
3) Oxygenated and substituted hydrocarbons from lignin pyrolysis
4) Nitromethane and other potential methyl radical oxidation products

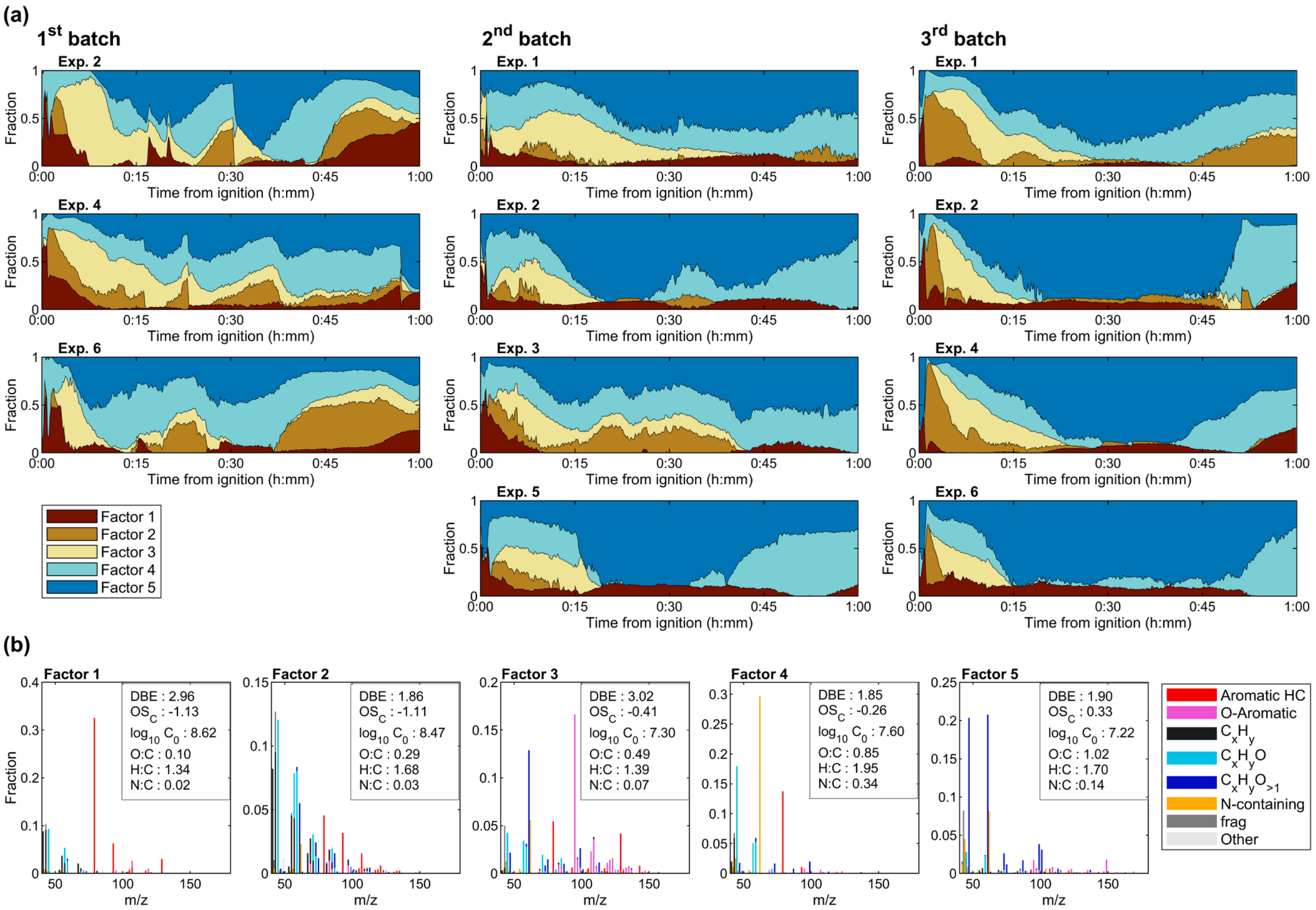

Fig. 4. The factorized composition of the exhaust (a) and the main factor characteristics and contribution of the ions to the total factor score (b). Note that the analysis was done for high-resolution data, but the spectra in (b) are illustrated in unit mass resolution for simplicity and ions at the same unit mass are stacked.

5) Products of fragmentation and recombination processes

The number of factors was decided based on the residuals, which did not exhibit a clear decrease with additional factors (Supplementary Figure S6). Further, introduction of the fifth factor separated the nitromethane-factor (Factor 4) and the mainly acidic fragmentation factor (Factor 5) while introduction of sixth factor led to no physically meaningful interpretations. The distribution of ions between each factor is illustrated in Fig. 5. The absolute factor concentrations and score values for these ions are shown in Supplementary Figures S7 and S8, respectively. The absolute score values for the ions are also available in Supplementary Table S3.

Factor 1 is an essentially hydrocarbonaceous, aromatic factor dominated by benzene. The formation of Factor 1 commenced instantly after batch addition, when the fresh fuel is heating up and begins pyrolyzing but is not encountered by a visible flame. This indicates that Factor 1 is related to the primary pyrolysis products. Factor 1 remained ubiquitous also during the later stages of combustion, suggesting that these compounds are produced from enduring fuel constituents and that these compounds are relatively stable at high combustion temperatures.

Factor 2 is composed of aliphatic hydrocarbons, such as propene, accompanied by small carbonyls, such as acetaldehyde and acetone/propanal. The formation of Factor 2 was initiated slightly after that of Factor 1, but was also particularly related to the ignition of the new batch. The time series of Factor 2 correlated with that of methanol (measured by FTIR; Pearson $r = 0.89$), which is considered a primary decomposition product from the methoxy groups in the fuel [25]. Factor 2 most closely followed the total OGC emission factor, peaking with the highest OGC emission at the ignition of a new batch, but also appearing when the emissions temporally increased in the middle of the batch. The presence of hydrocarbons implies occurrence of oxygen-poor areas leading to abstraction of oxygen-containing function groups. Factor 2 also encompasses a fraction of the ArHC, which may be either primary pyrolysis products or form via recombination of the smaller aliphatic precursors [25,27].

Factor 3 covers the majority of oxygenated aromatic emissions, and is proposed to entail the products of lignin-derived phenolic precursors. Factor 3 peaked shortly after ignition, but a few minutes after Factor 1, indicating that the decomposition of its precursors in the fuel required higher temperatures. Factor 3 was an important contributor to the total OGC emissions for roughly between 2 and 20 min from the ignition of a batch, signifying that lignin pyrolysis occurs within specific time frame. Previously, Kong et al. [28] separated products of cellulose and lignin combustion in combined gas and particle phases based on positive factor analysis of chemical ionization mass spectrometer data from residential wood combustion. They found the gaseous compounds in the lignin-related factor to increase briefly after ignition, similarly to Factor 3 of our study, while cellulose-derived products were contributing mainly to the particulate phase.

Factor 4 most notably encompasses $CH_3NO_2{-}H+$ and further comprises small carbonylic compounds, such as acetaldehyde, which are all products of the methyl radical oxidation in the presence of NO_x [66,67]. Based on the factor spectra, a fraction of benzene formation is also taking place simultaneously. The temporal dominance of this factor suggests that the conversion of the fuel nitrogen may influence the overall combustion kinetics during the batchwise brown coal

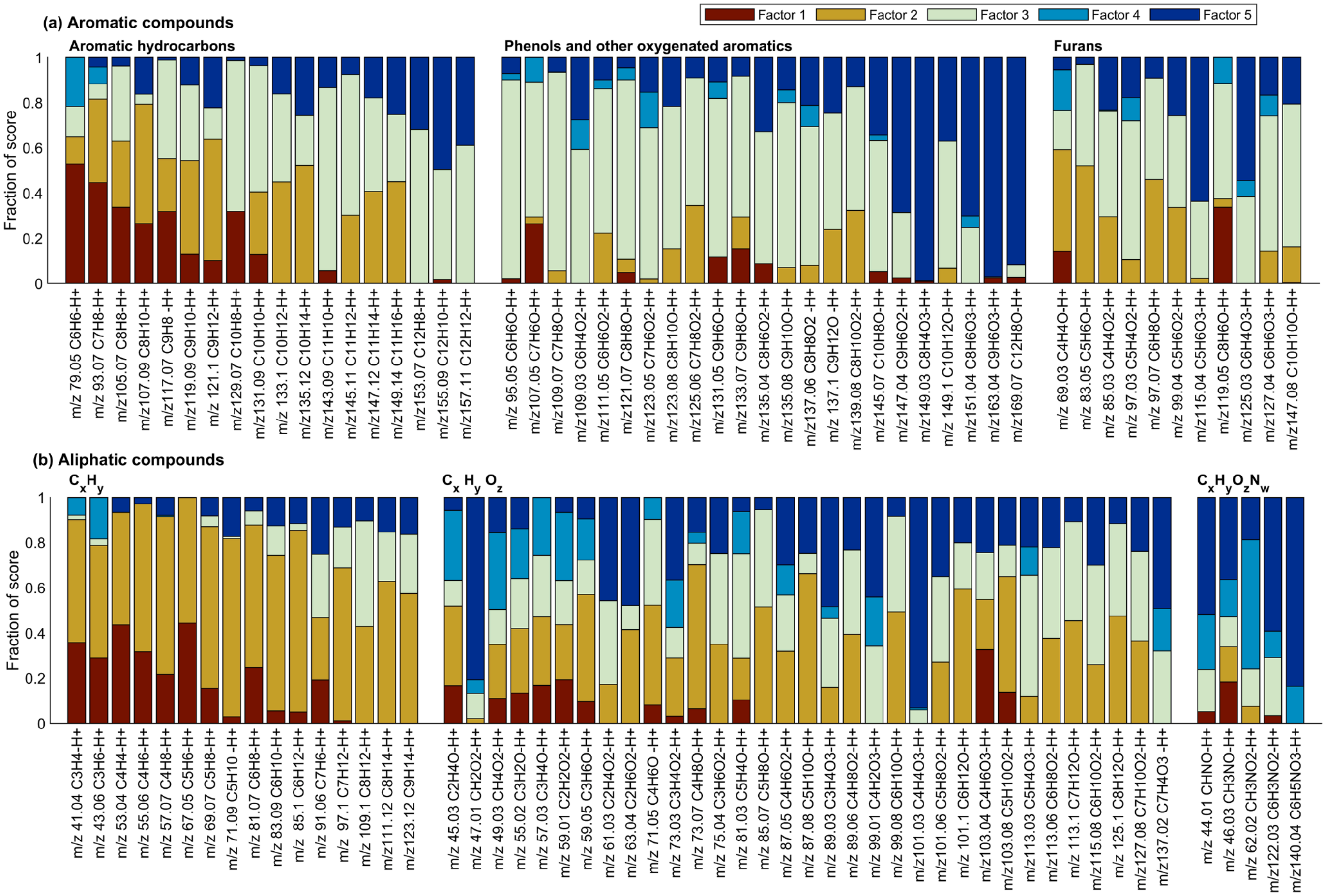

Fig. 5. Contribution of the five factors to the ion signals. Ions are presented as divided by functionality to aromatic (a) and aliphatic (b) compounds.

combustion process.

Factor 5 is most notably composed of small carboxylic acids such as formic acid (*m/z* 47.01) and acetic acid (*m/z* 61.03). A fraction of the C_{12}-PAHs formation was also allocated to this factor (Fig. 5). Thus, this factor can be considered related to high temperature conditions, where carboxylic acids are formed via thermal cracking and PAHs via recombination reactions [25]. Factor 5 typically formed the majority of the OGC emission in the middle of the batch (Fig. 4a), when other formation pathways were less dominant. Further, in higher combustion temperatures for example the phenolic lignin products of Factor 4 are deoxygenated, while larger species are formed via the enhanced hydrocarbon-abstraction-carbon-addition (HACA) reactions [25,26]. Such species are likely to have partitioned to the particle phase as soot or produce secondary gaseous species, which are visible in Factor 5. This agrees also with the previously observed temperature-dependance of PAH formation in coal combustion [77].

The factor analysis provides insight into the temporal variation of the combustion reactions. For example, the distribution of ArHC signals between the different factors exposes the several pathways for their formation (Fig. 5). Benzene and toluene were divided into Factors 1–4, portraying how in addition to being primary products of fuel pyrolysis, they are formed in the secondary processes in the flame and via recombination of smaller hydrocarbons. Conversely, naphthalene and methylnaphthalene were separated mainly into Factors 1 and 3, pointing towards their formation from the primary pyrolysis processes but also from phenolic precursors via cyclopentadiene or methylcyclopentadiene intermediates, respectively [26]. The observed C_{12}-PAHs, on the other hand, were connected solely to factors 3 and 5, indicating that their formation occurs either via the phenolic precursors (Factor 3) or by secondary recombination reactions in high-temperature flames (Factor 5). As the PTR-ToF did not distinguish between isomers, the division of each ion into the factors may also be influenced by variance in their respective composition.

4. Conclusions

Detailed emission factors were derived for organic gaseous emissions from residential-scale combustion of European brown coal briquettes. Of three subsequent batches of BCB combusted in a preheated stove, the first batch emitted significantly higher amounts of OGCs than the following batches. Relative composition of the different batches remained, however, distinctly similar. The presented emission factors confirm residential brown coal combustion as a potentially important local pollution source, even when the emissions were constrained by the briquetting of the brown coal, modern stove design with air-staging, and preheating of the stove. Furthermore, the OGCs from residential coal combustion were estimated to have notable secondary aerosol formation potential, as the approximated amount of photochemical SOA was roughly equivalent to the observed primary organic particle emission, while in dark conditions the oxygenated aromatic OGCs may have substantial potential for nitrophenol formation.

Although majority (92% as of 2020 [78]) of European brown coal is used for industrial scale power production, residential heating is likely to have disproportionally high impact on local air quality. The combustion conditions in power plants are more optimized, leading to more complete combustion and removal of the OGCs in the flue gases compared to residential appliances. Furthermore, power plants are typically equipped with highly efficient exhaust gas cleaning, whereas the lack of effective filtration remains an issue for small scale applications. The spectra of organic gaseous emissions from BCB combustion are closer to residential wood combustion than that of combustion of higher-ranking coals, which hinders source apportionment by gaseous tracers.

Factor analysis of high-resolution gas phase mass spectra proved to be a powerful tool for the study of the collective progression of solid fuel combustion. Information on the combustion processes could be distinguished even for the combustion of a complicated biomass-based fuel, where the interactions between different fuel constituents generally complicate the identification of underlying emission formation mechanisms. Temporal variation in the contributions of the five factors representing different OGC formation pathways reveal how the relative importance of the main fuel conversion and emission formation processes change depending on the combustion phase and the conditions existing within the batch. A distinct factor of oxygenated aromatics was related to the pyrolysis of the lignin residues in the brown coal, while single-ring and polycyclic aromatic hydrocarbons were connected to several factors and thus associated with both primary fuel pyrolysis and secondary recombination reactions.

Supporting information

Supporting Information contains detailed description of the bottom-up estimation on the SOA potential, additional information of the experimental conditions, and specifics on the analyzed compounds and NMF factorization. (pdf)

Novelty and significance statement

The organic gaseous emissions from residential brown combustion in European conditions are quantified in detail, providing important new information regarding these pollutants in urban air. Timeseries of organic gaseous emissions are assessed using a factor analysis approach, giving novel insight into the chemical processes governing fuel conversion and emission formation. A bottom-up investigation of the secondary organic particle formation potential of the emitted OGCs is performed in order to constrain the impact of residential combustion on European air quality. Results indicate notable influence of secondary particle formation to the total aerosol burden from residential brown coal combustion.

CRediT authorship contribution statement

Anni H. Hartikainen: Writing – review & editing, Writing – original draft, Visualization, Methodology, Investigation, Formal analysis, Data curation, Conceptualization. **Satish Basnet:** Writing – original draft, Investigation, Formal analysis, Data curation. **Pasi Yli-Pirilä:** Writing – original draft, Methodology, Investigation. **Mika Ihalainen:** Writing – original draft, Methodology, Investigation. **Sini Talvinen:** Writing – original draft, Validation, Methodology, Formal analysis. **Jarkko Tissari:** Writing – original draft, Resources, Methodology, Investigation. **Santtu Mikkonen:** Writing – original draft, Methodology, Formal analysis. **Ralf Zimmermann:** Supervision, Resources, Project administration, Funding acquisition, Conceptualization. **Olli Sippula:** Writing – review & editing, Writing – original draft, Supervision, Resources, Project administration, Methodology, Funding acquisition, Conceptualization, Investigation.

Declaration of competing interest

The authors declare that they have no known competing financial interests or personal relationships that could have appeared to influence the work reported in this paper.

Acknowledgements

Funding: This work was supported by the Research Council of Finland project BBrCAC [grant no. 341597] and the Helmholtz Virtual Institute of Complex Molecular Systems in Environmental Health - Aerosols and Health (HICE) funded by the Initiative and Networking Fund of the Helmholtz Association (HGF, Germany). S.M. is supported by the Research Council of Finland competitive funding to strengthen university research profiles (PROFI) for the University of Eastern Finland [grant no. 325022].

Supplementary materials

Supplementary material associated with this article can be found, in the online version, at doi:10.1016/j.combustflame.2024.113485.

References

[1] A. Kerimray, L. Rojas-Solórzano, M. Amouei Torkmahalleh, P.K. Hopke, B.P. Ó Gallachóir, Coal use for residential heating: patterns, health implications and lessons learned, Energy Sustain. Dev. 40 (2017) 19–30, https://doi.org/10.1016/j.esd.2017.05.005.

[2] T. Wiertz, L. Kuhn, A. Mattissek, A turn to geopolitics: shifts in the German energy transition discourse in light of Russia’s war against Ukraine, Energy Res. Soc. Sci. 98 (2023) 103036, https://doi.org/10.1016/j.erss.2023.103036.

[3] Y. Chen, G. Zhi, Y. Feng, D. Liu, G. Zhang, J. Li, G. Sheng, J. Fu, Measurements of black and organic carbon emission factors for household coal combustion in China: implication for emission reduction, Environ. Sci. Technol. 43 (2009) 9495–9500, https://doi.org/10.1021/es9021766.

[4] S. Cai, L. Zhu, S. Wang, A. Wisthaler, Q. Li, J. Jiang, J. Hao, Time-resolved intermediate-volatility and semivolatile organic compound emissions from household coal combustion in Northern China, Environ. Sci. Technol. 53 (2019) 9269–9278, https://doi.org/10.1021/acs.est.9b00734.

[5] K. He, Z. Shen, B. Zhang, J. Sun, H. Zou, M. Zhou, Z. Zhang, H. Xu, S.S.H. Ho, J. Cao, Emission profiles of volatile organic compounds from various geological maturity coal and its clean coal briquetting in China, Atmos. Res. 274 (2022), https://doi.org/10.1016/j.atmosres.2022.106200.

[6] F. Klein, S.M. Pieber, H. Ni, G. Stefenelli, A. Bertrand, D. Kilic, V. Pospisilova, B. Temime-Roussel, N. Marchand, I. El Haddad, J.G. Slowik, U. Baltensperger, J. Cao, R.J. Huang, A.S.H. Prévôt, Characterization of gas-phase organics using proton transfer reaction time-of-flight mass spectrometry: residential coal combustion, Environ. Sci. Technol. 52 (2018) 2612–2617, https://doi.org/10.1021/acs.est.7b03960.

[7] J. Sun, Z. Shen, L. Zhang, Y. Zhang, T. Zhang, Y. Lei, X. Niu, Q. Zhang, W. Dang, W. Han, J. Cao, H. Xu, P. Liu, X. Li, Volatile organic compounds emissions from traditional and clean domestic heating appliances in Guanzhong Plain, China: emission factors, source profiles, and effects on regional air quality, Environ. Int. (2019) 133, https://doi.org/10.1016/j.envint.2019.105252.

[8] T.C. Bond, D.S. Covert, J.C. Kramlich, T.V. Larson, R.J. Charlson, Primary particle emissions from residential coal burning: optical properties and size distributions, J. Geophys. Res. Atmos. 107 (2002), https://doi.org/10.1029/2001JD000571.

[9] Z. Qian, Y. Chen, Z. Liu, Y. Han, Y. Zhang, Y. Feng, Y. Shang, H. Guo, Q. Li, G. Shen, J. Chen, S. Tao, Intermediate volatile organic compound emissions from residential solid fuel combustion based on field measurements in rural China, Environ. Sci. Technol. 55 (2021) 5689–5700, https://doi.org/10.1021/acs.est.0c07908.

[10] Y. Wang, Y. Hou, H. Li, W. Wu, S. Ren, J. Li, New insights into the coalification of lignite from lignin: a comparison of their chemical structures, Fuel 326 (2022), https://doi.org/10.1016/j.fuel.2022.125017.

[11] D. Fabbri, L. Marynowski, M.J. Fabiańska, M. Zatoń, B.R.T. Simoneit, Levoglucosan and other cellulose markers in pyrolysates of miocene lignites: geochemical and environmental implications, Environ. Sci. Technol. 42 (2008) 2957–2963, https://doi.org/10.1021/es7021472.

[12] M. Rybicki, L. Marynowski, B.R.T. Simoneit, Composition of organic compounds from low-temperature burning of lignite and their application as tracers in ambient air, Chemosphere (2020) 249, https://doi.org/10.1016/j.chemosphere.2020.126087.

[13] J.M.K. O’Keefe, A. Bechtel, K. Christanis, S. Dai, W.A. DiMichele, C.F. Eble, J. S. Esterle, M. Mastalerz, A.L. Raymond, B.V. Valentim, N.J. Wagner, C.R. Ward, J. C. Hower, On the fundamental difference between coal rank and coal type, Int. J. Coal. Geol. 118 (2013) 58–87, https://doi.org/10.1016/j.coal.2013.08.007.

[14] K. Křůmal, P. Mikuška, J. Horák, F. Hopan, K. Krpec, Comparison of emissions of gaseous and particulate pollutants from the combustion of biomass and coal in modern and old-type boilers used for residential heating in the Czech Republic, Central Europe, Chemosphere 229 (2019) 51–59, https://doi.org/10.1016/j.chemosphere.2019.04.137.

[15] Y. Zhou, D. Huang, J. Lang, T. Zi, D. Chen, Y. Zhang, S. Li, Y. Jiao, S. Cheng, Improved estimation of rural residential coal emissions considering coal-stove combinations and combustion modes, Environ. Pollut. (2021) 272, https://doi.org/10.1016/j.envpol.2020.115558.

[16] C.H. Halios, C. Landeg-Cox, S.D. Lowther, A. Middleton, T. Marczylo, S. Dimitroulopoulou, Chemicals in European residences – Part I: a review of emissions, concentrations and health effects of volatile organic compounds (VOCs), Sci. Total Environ. 839 (2022), https://doi.org/10.1016/j.scitotenv.2022.156201.

[17] C.L. Heald, J.H. Kroll, The fuel of atmospheric chemistry: toward a complete description of reactive organic carbon, Sci. Adv. 6 (2020), https://doi.org/10.1126/sciadv.aay8967.

[18] A. Akherati, Y. He, M.M. Coggon, A.R. Koss, A.L. Hodshire, K. Sekimoto, C. Warneke, J. De Gouw, L. Yee, J.H. Seinfeld, T.B. Onasch, S.C. Herndon, W. B. Knighton, C.D. Cappa, M.J. Kleeman, C.Y. Lim, J.H. Kroll, J.R. Pierce, S. H. Jathar, Oxygenated aromatic compounds are important precursors of secondary organic aerosol in biomass-burning emissions, Environ. Sci. Technol. 54 (2020) 8568–8579, https://doi.org/10.1021/acs.est.0c01345.

[19] E.A. Bruns, I. El Haddad, J.G. Slowik, D. Kilic, F. Klein, U. Baltensperger, A.S. H. Prévôt, Identification of significant precursor gases of secondary organic aerosols from residential wood combustion, Sci. Rep. 6 (2016), https://doi.org/10.1038/srep27881.

[20] A. Hartikainen, P. Yli-Pirilä, P. Tiitta, A. Leskinen, M. Kortelainen, J. Orasche, J. Schnelle-Kreis, K.E.J. Lehtinen, R. Zimmermann, J. Jokiniemi, O. Sippula, Volatile organic compounds from logwood combustion: emissions and transformation under dark and photochemical aging conditions in a smog chamber, Environ. Sci. Technol. 52 (2018) 4979–4988, https://doi.org/10.1021/acs.est.7b06269.

[21] P. Martens, H. Czech, J. Tissari, M. Ihalainen, H. Suhonen, M. Sklorz, J. Jokiniemi, O. Sippula, R. Zimmermann, Emissions of gases and volatile organic compounds from residential heating: a comparison of brown coal briquettes and logwood combustion, Energy Fuels 35 (2021) 14010–14022, https://doi.org/10.1021/acs.energyfuels.1c01667.

[22] D.J. Lary, D.E. Shallcross, Central role of carbonyl compounds in atmospheric chemistry, J. Geophys. Res. Atmos. 105 (2000) 19771–19778, https://doi.org/10.1029/1999JD901184.

[23] G. McFiggans, T.F. Mentel, J. Wildt, I. Pullinen, S. Kang, E. Kleist, S. Schmitt, M. Springer, R. Tillmann, C. Wu, D. Zhao, M. Hallquist, C. Faxon, M. Le Breton, Å. M. Hallquist, D. Simpson, R. Bergström, M.E. Jenkin, M. Ehn, J.A. Thornton, M. R. Alfarra, T.J. Bannan, C.J. Percival, M. Priestley, D. Topping, A. Kiendler-Scharr, Secondary organic aerosol reduced by mixture of atmospheric vapours, Nature 565 (2019) 587–593, https://doi.org/10.1038/s41586-018-0871-y.

[24] K.N. Rowell, S.H. Kable, M.J.T. Jordan, An assessment of the tropospherically accessible photo-initiated ground state chemistry of organic carbonyls, Atmos. Chem. Phys. 22 (2022), https://doi.org/10.5194/acp-22-929-2022.

[25] F.X. Collard, J. Blin, A review on pyrolysis of biomass constituents: mechanisms and composition of the products obtained from the conversion of cellulose, hemicelluloses and lignin, Renew. Sustain. Energy Rev. 38 (2014), https://doi.org/10.1016/j.rser.2014.06.013.

[26] E.M. Fitzpatrick, J.M. Jones, M. Pourkashanian, A.B. Ross, A. Williams, K.D. Bartle, Mechanistic aspects of soot formation from the combustion of pine wood, Energy Fuels 22 (2008), https://doi.org/10.1021/ef800456k.

[27] J. Warnatz, Hydrocarbon oxidation high-temperature chemistry, Pure Appl. Chem 72 (2000) 2101–2110, https://doi.org/10.1351/pac200072112101.

[28] X. Kong, C.M. Salvador, S. Carlsson, R. Pathak, K.O. Davidsson, M. Le Breton, S. M. Gaita, K. Mitra, Å.M. Hallquist, M. Hallquist, J.B.C. Pettersson, Molecular characterization and optical properties of primary emissions from a residential wood burning boiler, Sci. Total Environ. 754 (2021), https://doi.org/10.1016/j.scitotenv.2020.142143.

[29] K. Sekimoto, A.R. Koss, J.B. Gilman, V. Selimovic, M.M. Coggon, K.J. Zarzana, B. Yuan, B.M. Lerner, S.S. Brown, C. Warneke, R.J. Yokelson, J.M. Roberts, J. De Gouw, High-and low-temperature pyrolysis profiles describe volatile organic compound emissions from western US wildfire fuels, Atmos. Chem. Phys. 18 (2018), https://doi.org/10.5194/acp-18-9263-2018.

[30] F.Y. Majluf, J.E. Krechmer, C. Daube, W.B. Knighton, C. Dyroff, A.T. Lambe, E. C. Fortner, T.I. Yacovitch, J.R. Roscioli, S.C. Herndon, D.R. Worsnop, M. R. Canagaratna, Mobile near-field measurements of biomass burning volatile organic compounds: emission ratios and factor analysis, Environ. Sci. Technol. Lett. (2022), https://doi.org/10.1021/acs.estlett.2c00194.

[31] H. Czech, O. Sippula, M. Kortelainen, J. Tissari, C. Radischat, J. Passig, T. Streibel, J. Jokiniemi, R. Zimmermann, On-line analysis of organic emissions from residential wood combustion with single-photon ionisation time-of-flight mass spectrometry (SPI-TOFMS), Fuel 177 (2016) 334–342, https://doi.org/10.1016/j.fuel.2016.03.036.

[32] J.B. Pernov, R. Bossi, T. Lebourgeois, J.K. Nøjgaard, R. Holzinger, J.L. Hjorth, H. Skov, Atmospheric VOC measurements at a High Arctic site: characteristics and source apportionment, Atmos. Chem. Phys. 21 (2021), https://doi.org/10.5194/acp-21-2895-2021.

[33] Z. Zhang, H. Man, L. Qi, X. Wang, H. Liu, J. Zhao, H. Wang, S. Jing, T. He, S. Wang, K. He, Measurement and minutely-resolved source apportionment of ambient VOCs in a corridor city during 2019 China International Import Expo episode, Sci. Total Environ. 798 (2021), https://doi.org/10.1016/j.scitotenv.2021.149375.

[34] R. Yadav, L.K. Sahu, N. Tripathi, D. Pal, G. Beig, S.N.A. Jaaffrey, Investigation of emission characteristics of NMVOCs over urban site of western India, Environ. Pollut. 252 (2019), https://doi.org/10.1016/j.envpol.2019.05.089.

[35] G.I. Gkatzelis, M.M. Coggon, B.C. McDonald, J. Peischl, J.B. Gilman, K.C. Aikin, M. A. Robinson, F. Canonaco, A.S.H. Prevot, M. Trainer, C. Warneke, Observations confirm that volatile chemical products are a major source of petrochemical emissions in U.S. Cities, Environ. Sci. Technol. 55 (2021), https://doi.org/10.1021/acs.est.0c05471.

[36] H. Li, M.R. Canagaratna, M. Riva, P. Rantala, Y. Zhang, S. Thomas, L. Heikkinen, P. M. Flaud, E. Villenave, E. Perraudin, D. Worsnop, M. Kulmala, M. Ehn, F. Bianchi, Atmospheric organic vapors in two European pine forests measured by a Vocus PTR-TOF: insights into monoterpene and sesquiterpene oxidation processes, Atmos. Chem. Phys. 21 (2021), https://doi.org/10.5194/acp-21-4123-2021.

[37] V. Leinonen, P. Tiitta, O. Sippula, H. Czech, A. Leskinen, S. Isokääntä, J. Karvanen, S. Mikkonen, Modeling atmospheric aging of small-scale wood combustion emissions: distinguishing causal effects from non-causal associations, Environ. Sci. Atmos. 2 (2022), https://doi.org/10.1039/d2ea00048b.

[38] P. Martens, H. Czech, J. Orasche, G. Abbaszade, M. Sklorz, B. Michalke, J. Tissari, T. Bizjak, M. Ihalainen, H. Suhonen, P. Yli-Pirilä, J. Jokiniemi, O. Sippula, R. Zimmermann, Brown coal and logwood combustion in a modern heating appliance: the impact of combustion quality and fuel on organic aerosol composition, Environ. Sci. Technol. (2023), https://doi.org/10.1021/acs.est.2c08787.

[39] A. Hartikainen, P. Tiitta, M. Ihalainen, P. Yli-Pirilä, J. Orasche, H. Czech, M. Kortelainen, H. Lamberg, H. Suhonen, H. Koponen, L. Hao, R. Zimmermann, J. Jokiniemi, J. Tissari, O. Sippula, Photochemical transformation of residential wood combustion emissions: dependence of organic aerosol composition on OH exposure, Atmos. Chem. Phys. 20 (2020), https://doi.org/10.5194/acp-20-6357-2020.

[40] T. Ihantola, M.R. Hirvonen, M. Ihalainen, H. Hakkarainen, O. Sippula, J. Tissari, S. Bauer, S. Di Bucchianico, N. Rastak, A. Hartikainen, J. Leskinen, P. Yli-Pirilä, M. V. Martikainen, M. Miettinen, H. Suhonen, T.J. Rönkkö, M. Kortelainen, H. Lamberg, H. Czech, P. Martens, J. Orasche, B. Michalke, A.Ö. Yildirim, J. Jokiniemi, R. Zimmermann, P.I. Jalava, Genotoxic and inflammatory effects of spruce and brown coal briquettes combustion aerosols on lung cells at the air-liquid interface, Sci. Total Environ. 806 (2022), https://doi.org/10.1016/j.scitotenv.2021.150489.

[41] A. Jordan, S. Haidacher, G. Hanel, E. Hartungen, L. Märk, H. Seehauser, R. Schottkowsky, P. Sulzer, T.D. Märk, A high resolution and high sensitivity proton-transfer-reaction time-of-flight mass spectrometer (PTR-TOF-MS), Int. J. Mass Spectrom. 286 (2009) 122–128, https://doi.org/10.1016/j.ijms.2009.07.005.

[42] L. Cappellin, T. Karl, M. Probst, O. Ismailova, P.M. Winkler, C. Soukoulis, E. Aprea, T.D. Märk, F. Gasperi, F. Biasioli, On quantitative determination of volatile organic compound concentrations using proton transfer reaction time-of-flight mass spectrometry, Environ. Sci. Technol. 46 (2012) 2283–2290, https://doi.org/10.1021/es203985t.

[43] K. Buhr, S. van Ruth, C. Delahunty, Analysis of volatile flavour compounds by Proton Transfer Reaction-Mass Spectrometry: fragmentation patterns and discrimination between isobaric and isomeric compounds, Int. J. Mass Spectrom. 221 (2002) 1–7, https://doi.org/10.1016/S1387-3806(02)00896-5.

[44] M. Gueneron, M.H. Erickson, G.S. Vanderschelden, B.T. Jobson, PTR-MS fragmentation patterns of gasoline hydrocarbons, Int. J. Mass Spectrom. 379 (2015) 97–109, https://doi.org/10.1016/j.ijms.2015.01.001.

[45] B.T. Jobson, R.A. Volkamer, E. Velasco, G. Allwine, H. Westberg, B.K. Lamb, M. L. Alexander, C.M. Berkowitz, L.T. Molina, Comparison of aromatic hydrocarbon measurements made by PTR-MS, DOAS and GC-FID during the MCMA 2003 field experiment, Atmos. Chem. Phys. 10 (2010) 1989–2005, https://doi.org/10.5194/acp-10-1989-2010.

[46] Y. Li, U. Pöschl, M. Shiraiwa, Molecular corridors and parameterizations of volatility in the chemical evolution of organic aerosols, Atmos. Chem. Phys. 16 (2016) 3327–3344, https://doi.org/10.5194/acp-16-3327-2016.

[47] J.H. Kroll, N.M. Donahue, J.L. Jimenez, S.H. Kessler, M.R. Canagaratna, K. R. Wilson, K.E. Altieri, L.R. Mazzoleni, A.S. Wozniak, H. Bluhm, E.R. Mysak, J. D. Smith, C.E. Kolb, D.R. Worsnop, Carbon oxidation state as a metric for describing the chemistry of atmospheric organic aerosol, Nat. Chem. 3 (2011) 133–139, https://doi.org/10.1038/nchem.948.

[48] European Environment Agency, Air quality in Europe 2022, 2022. https://doi.org/10.2800/049755.

[49] M. Hallquist, J.C. Wenger, U. Baltensperger, Y. Rudich, D. Simpson, M. Claeys, J. Dommen, N.M. Donahue, C. George, A.H. Goldstein, J.F. Hamilton, H. Herrmann, T. Hoffmann, Y. Iinuma, M. Jang, M.E. Jenkin, J.L. Jimenez, A. Kiendler-Scharr, W. Maenhaut, G. Mcfiggans, T.F. Mentel, A. Monod, A.S. H. Prévôt, J.H. Seinfeld, J.D. Surratt, R. Szmigielski, J. Wildt, The formation, properties and impact of secondary organic aerosol: current and emerging issues, Atmos. Chem. Phys 9 (2009) 5155–5236, https://doi.org/10.5194/acp-9-5155-2009.

[50] E. Kari, L. Hao, P. Yli-Pirilä, A. Leskinen, M. Kortelainen, J. Grigonyte, D. R. Worsnop, J. Jokiniemi, O. Sippula, C.L. Faiola, A. Virtanen, Effect of pellet boiler exhaust on secondary organic aerosol formation from α-Pinene, Environ. Sci. Technol. 51 (2017) 1423–1432, https://doi.org/10.1021/acs.est.6b04919.

[51] X. Jiang, N.T. Tsona, L. Jia, S. Liu, H. Zhang, Y. Xu, L. Du, Secondary organic aerosol formation from photooxidation of furan: effects of NOx and humidity, Atmos. Chem. Phys. 19 (2019) 13591–13609, https://doi.org/10.5194/acp-19-13591-2019.

[52] J. Dommen, A. Metzger, J. Duplissy, M. Kalberer, M.R. Alfarra, A. Gascho, E. Weingartner, A.S.H. Prevot, B. Verheggen, U. Baltensperger, Laboratory observation of oligomers in the aerosol from isoprene/NOx photooxidation, Geophys. Res. Lett. 33 (2006) L13805, https://doi.org/10.1029/2006GL026523.

[53] R.M. Healy, B. Temime, K. Kuprovskyte, J.C. Wenger, Effect of relative humidity on gas/particle partitioning and aerosol mass yield in the photooxidation of p-xylene, Environ. Sci. Technol. 43 (2009) 1884–1889, https://doi.org/10.1021/es802404z.

[54] D.D. Lee, H.S. Seung, Learning the parts of objects by non-negative matrix factorization, Nature 401 (1999) 788–791, https://doi.org/10.1038/44565.

[55] S. Isokääntä, E. Kari, A. Buchholz, L. Hao, S. Schobesberger, A. Virtanen, S. Mikkonen, Comparison of dimension reduction techniques in the analysis of mass spectrometry data, Atmos. Meas. Tech. 13 (2020) 2995–3022, https://doi.org/10.5194/amt-13-2995-2020.

[56] M.W. Berry, M. Browne, A.N. Langville, V.P. Pauca, R.J. Plemmons, Algorithms and applications for approximate nonnegative matrix factorization, Comput. Stat. Data Anal. 52 (2007) 155–173, https://doi.org/10.1016/j.csda.2006.11.006.

[57] G.J. Stewart, W.J.F. Acton, B.S. Nelson, A.R. Vaughan, J.R. Hopkins, R. Arya, A. Mondal, R. Jangirh, S. Ahlawat, L. Yadav, S.K. Sharma, R.E. Dunmore, S.S. M. Yunus, C.Nicholas Hewitt, E. Nemitz, N. Mullinger, R. Gadi, L.K. Sahu, N. Tripathi, A.R. Rickard, J.D. Lee, T.K. Mandal, J.F. Hamilton, Emissions of non-methane volatile organic compounds from combustion of domestic fuels in Delhi, India, Atmos. Chem. Phys. 21 (2021) 2383–2406, https://doi.org/10.5194/acp-21-2383-2021.

[58] European Environment Agency, EMEP/EEA air pollutant emission inventory guidebook 2019. Tech. Guid. Prepare Natl. Emission Inventories, 2019, https://doi.org/10.2800/293657.

[59] M. Savolahti, N. Karvosenoja, S. Soimakallio, K. Kupiainen, J. Tissari, V.V. Paunu, Near-term climate impacts of Finnish residential wood combustion, Energy Policy (2019) 133, https://doi.org/10.1016/j.enpol.2019.06.045.

[60] E.A. Bruns, J.G. Slowik, I. El Haddad, D. Kilic, F. Klein, J. Dommen, B. Temime-Roussel, N. Marchand, U. Baltensperger, A.S.H. Prévôt, Characterization of gas-phase organics using proton transfer reaction time-of-flight mass spectrometry: fresh and aged residential wood combustion emissions, Atmos. Chem. Phys. 17 (2017), https://doi.org/10.5194/acp-17-705-2017.

[61] E.M. Fitzpatrick, A.B. Ross, J. Bates, G. Andrews, J.M. Jones, H. Phylaktou, M. Pourkashanian, A. Williams, Emission of oxygenated species from the combustion of pine wood and its relation to soot formation, Process Saf. Environ. Protect. 85 (2007), https://doi.org/10.1205/psep07020.

[62] K.O. Johansson, T. Dillstrom, M. Monti, F. El Gabaly, M.F. Campbell, P.E. Schrader, D.M. Popolan-Vaida, N.K. Richards-Henderson, K.R. Wilson, A. Violi, H. A. Michelsen, Formation and emission of large furans and oxygenated hydrocarbons from flames, Proc. Natl. Acad. Sci. u S. a 113 (2016), https://doi.org/10.1073/pnas.1604772113.

[63] J.B. Gilman, B.M. Lerner, W.C. Kuster, P.D. Goldan, C. Warneke, P.R. Veres, J. M. Roberts, J.A. De Gouw, I.R. Burling, R.J. Yokelson, Biomass burning emissions and potential air quality impacts of volatile organic compounds and other trace gases from fuels common in the US, Atmos. Chem. Phys. 15 (2015), https://doi.org/10.5194/acp-15-13915-2015.

[64] K.P. Shrestha, L. Seidel, T. Zeuch, G. Moréac, P. Dagaut, F. Mauss, On the implications of nitromethane – NOx chemistry interactions for combustion processes, Fuel (2021) 289, https://doi.org/10.1016/j.fuel.2020.119861.

[65] S. Inomata, H. Tanimoto, Y. Fujitani, K. Sekimoto, K. Sato, A. Fushimi, H. Yamada, S. Hori, Y. Kumazawa, A. Shimono, T. Hikida, On-line measurements of gaseous nitro-organic compounds in diesel vehicle exhaust by proton-transfer-reaction mass spectrometry, Atmos. Environ. 73 (2013) 195–203, https://doi.org/10.1016/j.atmosenv.2013.03.035.

[66] K.P. Shrestha, B.R. Giri, M. Adil, L. Seidel, T. Zeuch, A. Farooq, F. Mauss, Detailed chemical kinetic study of acetaldehyde oxidation and its interaction with NOx, Energy Fuels 35 (2021) 14963–14983, https://doi.org/10.1021/acs.energyfuels.1c01948.

[67] F.E. Alam, F.M. Haas, T.I. Farouk, F.L. Dryer, Influence of trace nitrogen oxides on natural gas oxidation: flow reactor measurements and kinetic modeling, Energy Fuels 31 (2017) 2360–2369, https://doi.org/10.1021/acs.energyfuels.6b02369.

[68] K. He, T. Fu, B. Zhang, H. Xu, J. Sun, H. Zou, Z. Zhang, S.S. Hang Ho, J. Cao, Z. Shen, Examination of long-time aging process on volatile organic compounds emitted from solid fuel combustion in a rural area of China, Chemosphere (2023) 333, https://doi.org/10.1016/j.chemosphere.2023.138957.

[69] Z.C.J. Decker, M.A. Robinson, K.C. Barsanti, I. Bourgeois, M.M. Coggon, J. P. Digangi, G.S. Diskin, F.M. Flocke, A. Franchin, C.D. Fredrickson, G.I. Gkatzelis, S.R. Hall, H. Halliday, C.D. Holmes, L.G. Huey, Y.R. Lee, J. Lindaas, A. M. Middlebrook, D.D. Montzka, R. Moore, J.A. Neuman, J.B. Nowak, B.B. Palm, J. Peischl, F. Piel, P.S. Rickly, A.W. Rollins, T.B. Ryerson, R.H. Schwantes, K. Sekimoto, L. Thornhill, J.A. Thornton, G.S. Tyndall, K. Ullmann, P. Van Rooy, P. R. Veres, C. Warneke, R.A. Washenfelder, A.J. Weinheimer, E. Wiggins, E. Winstead, A. Wisthaler, C. Womack, S.S. Brown, Nighttime and daytime dark oxidation chemistry in wildfire plumes: an observation and model analysis of FIREX-AQ aircraft data, Atmos. Chem. Phys. 21 (2021) 16293–16317, https://doi.org/10.5194/acp-21-16293-2021.

[70] E. Bolzacchini, M. Bruschi, J. Hjorth, S. Meinardi, M. Orlandi, B. Rindone, E. Rosenbohm, Gas-phase reaction of phenol with NO3, Environ. Sci. Technol. 35 (2001), https://doi.org/10.1021/es001290m.

[71] Z.C.J. Decker, K.J. Zarzana, M. Coggon, K.E. Min, I. Pollack, T.B. Ryerson, J. Peischl, P. Edwards, W.P. Dubé, M.Z. Markovic, J.M. Roberts, P.R. Veres, M. Graus, C. Warneke, J. De Gouw, L.E. Hatch, K.C. Barsanti, S.S. Brown, Nighttime chemical transformation in biomass burning plumes: a box model analysis initialized with aircraft observations, Environ. Sci. Technol. 53 (2019) 2529–2538, https://doi.org/10.1021/acs.est.8b05359.

[72] R.J. Mayorga, Z. Zhao, H. Zhang, Formation of secondary organic aerosol from nitrate radical oxidation of phenolic VOCs: implications for nitration mechanisms and brown carbon formation, Atmos. Environ. 244 (2021), https://doi.org/10.1016/j.atmosenv.2020.117910.

[73] T.J. Bannan, A.M. Booth, B.T. Jones, S. O'Meara, M.H. Barley, I. Riipinen, C. J. Percival, D. Topping, Measured saturation vapor pressures of phenolic and nitro-aromatic compounds, Environ. Sci. Technol. 51 (2017), https://doi.org/10.1021/acs.est.6b06364.

[74] C.D. Fredrickson, B.B. Palm, B.H. Lee, X. Zhang, J.J. Orlando, G.S. Tyndall, L. A. Garofalo, M.A. Pothier, D.K. Farmer, Z.C.J. Decker, M.A. Robinson, S.S. Brown, S.M. Murphy, Y. Shen, A.P. Sullivan, S. Schobesberger, J.A. Thornton, Formation and evolution of catechol-derived SOA mass, composition, volatility, and light absorption, ACS. Earth. Space Chem. 6 (2022), https://doi.org/10.1021/acsearthspacechem.2c00007.

[75] C. Li, Q. He, A.P.S. Hettiyadura, U. Käfer, G. Shmul, D. Meidan, R. Zimmermann, S. S. Brown, C. George, A. Laskin, Y. Rudich, Formation of secondary brown carbon in biomass burning aerosol proxies through no3 radical reactions, Environ. Sci. Technol. 54 (2020), https://doi.org/10.1021/acs.est.9b05641.

[76] C. Lu, X. Wang, R. Li, R. Gu, Y. Zhang, W. Li, R. Gao, B. Chen, L. Xue, W. Wang, Emissions of fine particulate nitrated phenols from residential coal combustion in China, Atmos. Environ. 203 (2019) 10–17, https://doi.org/10.1016/j.atmosenv.2019.01.047.

[77] M. Gao, Y. Wang, J. Dong, F. Li, K. Xie, Release behavior and formation mechanism of polycyclic aromatic hydrocarbons during coal pyrolysis, Chemosphere 158 (2016), https://doi.org/10.1016/j.chemosphere.2016.05.024.

[78] Eurostat, Coal production and consumption statistics, Stat. Explained (2022). https://ec.europa.eu/eurostat/statistics-explained/index.php?title=Coal_production_and_consumption_statistics#Consumption_and_production_of_brown_coal (accessed June 7, 2023).